



Showcasing research from the Multifunctional Optical Materials group at the Institute of Materials Science of Seville, Spain.

Determination of the optical constants of ligand-free organic lead halide perovskite quantum dots

Herein we demonstrate a method to determine the complex refractive index of MAPbBr_3 and MAPbI_3 perovskite quantum dots (QDs). We take advantage of a scaffold-based, ligand-free, synthetic approach that gives rise to transparent composite films that allow a clean analysis of the QD optical constants, without the interference of organic layers. These results may be used to achieve a finer design and optimization of perovskite quantum dot optoelectronic devices.

As featured in:



See Hernán Míguez *et al.*, *Nanoscale*, 2023, 15, 2553.


 Cite this: *Nanoscale*, 2023, **15**, 2553

Received 16th September 2022,

Accepted 1st November 2022

DOI: 10.1039/d2nr05109e

rsc.li/nanoscale

Determination of the optical constants of ligand-free organic lead halide perovskite quantum dots†

 Andrea Rubino, Gabriel Lozano, Mauricio E. Calvo  and Hernán Míguez *

Precise knowledge of the optical constants of perovskite lead halide quantum dots (QDs) is required to both understand their interaction with light and to rationally design and optimize the devices based on them. However, their determination from colloidal nanocrystal suspensions, or films made out of them, remains elusive, as a result of the difficulty in disentangling the optical constants of the organic capping ligands and those of the semiconductor itself. In this work, we extract the refractive index and extinction coefficient of ligand-free methylammonium lead iodide (MAPbI₃) and bromide (MAPbBr₃) nanocrystals. In order to prevent the use of organic ligands in the preparation, we follow a scaffold assisted synthetic procedure, which yields a composite film of high optical quality that can be independently and precisely characterized and modelled. In this way, the contribution of the guest nanocrystals can be successfully discriminated from that of the host matrix. Using a Kramers–Kronig consistent dispersion model along with an effective medium approximation, it is possible to derive the optical constants of the QDs by fitting the spectral dependence of light transmitted and reflected at different angles and polarizations. Our results indicate a strong dependence of the optical constants on the QD size. Small nanocrystals show remarkably large values of the extinction coefficient compared to their bulk counterparts. This analysis opens the door to the rigorous modelling of solar cells and light-emitting diodes with active layers based on perovskite QDs.

Introduction

The determination of the optical constants (*i.e.*, refractive index and extinction coefficient) of semiconductors is essential

to model their interaction with light, which is also central to the optimization of the performance of optoelectronic devices. They are typically determined from the analysis of the optical response of the materials with the aid of appropriate models.^{1–8} As far as lead halide perovskites are concerned, several studies have focused on the characterization of their optical constants.^{8–17} Remarkably, a comparative analysis reveals that significant dispersion is observed for materials that are nominally the same, which is mainly attributed to differences in sample preparation.¹⁸ As far as we know, to date, all reported works have focused on the analysis of the optical constants of perovskites in the shape of thin films or single crystals. However, the determination of the complex refractive index of perovskite nanocrystals remains elusive. This contrasts with their relevance in different applied research fields, such as light-emitting diodes,^{19,20} solar cells,^{21,22} transistors,²³ photodetectors²⁴ and, more recently, X-ray detection,²⁵ or non-linear optics,^{26,27} which could greatly benefit from optimized designs that require a precise knowledge of the optical constants of all materials involved, as it has been demonstrated for their bulk counterparts.^{15,16,28}

In order to perform a reliable determination of the optical constants of a material, uniform and scattering-free films are required. However, the preparation of such films out of colloidal nanocrystals, which are typically attained by ligand-assisted synthesis,^{29,30} is not straightforward. Furthermore, the structural configuration of the ligand network in a film made of colloidal nanocrystals is strongly dependent on the interaction between them, which depends in turn on the processing of the sample. So, even if high quality films can be obtained, since both sets of optical constants (*i.e.*, that of the nanocrystals and the one corresponding to the ligand network) are unknown, discriminating between their relative contributions to the overall optical response of a quantum dot solid is not an easy task.^{31–34} On the other hand, it has been recently demonstrated that optoelectronic quality perovskite QDs can be achieved within the void network of pore size controlled metal oxide matrices.³⁵ Moreover, these can be made in

Instituto de Ciencia de Materiales de Sevilla (CSIC-US), C/Américo Vespucio 49, 41092 Sevilla, Spain. E-mail: h.miguez@csic.es

† Electronic supplementary information (ESI) available: Details of the Tauc plot analysis; the use of the Brus equation; the experimental quantification of the QD filling fraction; the modeling of the complex refractive index; the extracted dielectric constants; the comparison between different effective medium approximations. See DOI: <https://doi.org/10.1039/d2nr05109e>



the shape of homogeneous and uniform scattering-free films,^{36,37} which opens the possibility to perform specular reflection and ballistic transmission measurements that allow a precise estimation of their average optical constants as reliable as those attained by ellipsometry characterization.^{38,39} Since in this case both the optical constants and the volume fraction of the host are known, it may be possible to differentiate the contribution from the semiconductor nanocrystals and determine their optical constants in a reliable way.

Based on this hypothesis, in this work we obtain the optical constants of ligand-free MAPbI₃ and MAPbBr₃ QDs embedded in porous scaffolds. The transparent porous films employed as hosts provide the necessary environmental stability required to perform reliable characterization of their optical properties without the need for ligands. A combination of a Forouhi-Bloomer model, employed to describe the spectral dependence of the complex refractive index of the QDs, and an effective medium approximation, accounting for the interaction between perovskite NCs and the porous silica matrix, is employed to fit the optical reflectance and transmittance measured at different angles from a series of QD embedded films⁴⁰ and extract their optical constants. Interestingly, our analysis reveals that QD size reduction brings about an increase in the extinction coefficient. Our results not only provide information on the fundamental constants of nano-sized organic lead halides, but also open the door to precise modelling of perovskite QD-based optoelectronic devices.

Results and discussion

Nanocrystal synthesis and characterization

Porous silicon oxide films exhibiting plane-parallel interfaces and a high transparency, with a thickness d of ~ 400 nm, were used as scaffolds for the synthesis of MAPbBr₃ and MAPbI₃ QDs analyzed in this work, following a procedure thoroughly described before.³⁷ Fig. 1(a and b) show the transmission electron microscopy (TEM) images of these films. Fig. 1c shows a typical TEM cross section of a focused ion beam cleaved and thinned lamella of a quantum dot filled porous silica scaffold (QD-MAPbBr₃@SiO₂) film, in which the semiconductor nanocrystals can be identified as dark spots inside the matrix. X-ray diffractograms confirm the presence of perovskite crystallites, as illustrated in Fig. 1d, with the main peaks associated with bromide- and iodide-based perovskites being clearly observed around $2\theta = 14.9^\circ$ and $2\theta = 14.1^\circ$, respectively.⁴¹ Fig. 2 shows the corresponding photoluminescence (PL) spectra recorded from QD-MAPbBr₃@SiO₂ (Fig. 2a) and QD-MAPbI₃@SiO₂ (Fig. 2b). The PL spectra of the thin films of the bulk perovskite materials are also shown in Fig. 2a and b, for the sake of comparison. The characteristic gradual blue-shift of the electronic band gap is observed as the size of either MAPbI₃ or MAPbBr₃ nanocrystals becomes smaller. The average QD diameters were estimated both from the analysis of HRTEM images and by fitting the spectral position of the luminescence peak to the Brus model,⁴² which offer consistent results (full



Fig. 1 (a and b) High-resolution TEM micrographs of MAPbBr₃ (a) and MAPbI₃ (b) nanocrystals inside a porous silica matrix. (c) The TEM cross section of the QD-MAPbBr₃@SiO₂ composite layer. (d) XRD diffractograms of QD-MAPbBr₃@SiO₂ (green line) and QD-MAPbI₃@SiO₂ (red line). For the sake of clarity, backgrounds were subtracted in both diffractograms.

details of the fittings can be found in the ESI†). The absorbance of these films was also estimated by measuring the total reflectance (R_T) and transmittance (T_T), and according to the formula $A = 1 - R_T - T_T$. Fig. 2c and d show the Tauc plots obtained for the different samples, which allow us to estimate the band gap energy (E_g) plotted versus the QD diameters in Fig. 2e and f.^{43,44} A maximum blue-shift of ~ 100 meV is observed for the smallest QDs synthesized with respect to the E_g of the bulk materials in each case.

Determination of the optical constants

In order to extract the optical constants of the QDs, we measured the spectral dependence of light reflected and transmitted at different angles for both polarizations of the incident beam and fitted it using a model based on the transfer matrix formalism.¹⁵ This method, which has been successfully employed in recent years to calculate the optical constants of homogeneous ABX₃ perovskite films or single crystals, constitutes a robust alternative to ellipsometry,^{15,39} and has been applied to optimize the photo-conversion performance of high-efficient perovskite solar cells prepared by solution processing or evaporation.^{16,28} In the present work, our model considers a system composed of a thin film (the porous silica matrix loaded with QDs) characterized by a thickness d and a



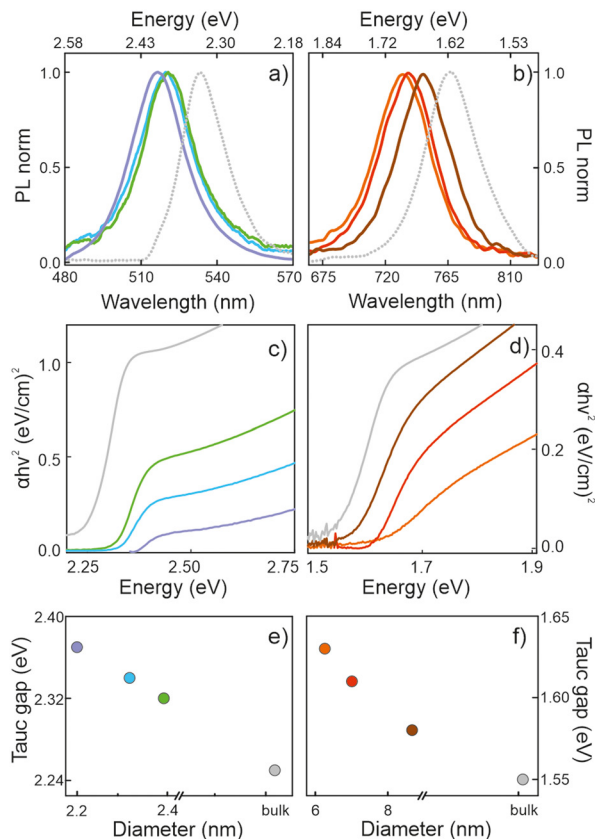


Fig. 2 (a and b) The normalized PL spectra of MAPbBr₃ (a) and MAPbI₃ (b) QDs dispersed inside the porous films. All emissions were blue-shifted with respect to the spectral position of the bulk emission (grey dashed lines). (c) The Tauc plots of the MAPbBr₃@SiO₂ films, where the nanocrystal sizes are 2.4 nm (green line), 2.3 nm (blue line) and 2.2 nm (violet line). (d) The Tauc plots of the MAPbI₃@SiO₂ films, where the nanocrystal sizes are 9 nm (brown line), 7 nm (red line) and 6 nm (orange line). Grey lines represent the Tauc plots of the respective bulk films. (d and e) Size dependence of the Tauc gap (E_g extracted from the Tauc plots) for the MAPbBr₃ (e) and MAPbI₃ (f) QDs (color code as in (c) and (d)).

complex effective refractive index, $N_{\text{eff}} = n + ik$. A substrate of a refractive index 1.51 and thickness 1 mm is also assumed, while air is taken as the incoming and outgoing medium. In order to calculate the real (n) and imaginary (k) parts of N_{eff} , we use the approach developed by Maxwell and Garnett (MG), a well-established effective medium approximation that has been successfully employed recently to attain the N_{eff} of colloidal quantum dot solid films.³¹ In our case, both pores and perovskite nanocrystals are considered inclusions in the silica matrix.⁴⁵ For the calculations, we first experimentally determined the volume filling fractions of both the porous scaffold (ff_{SiO_2}) and the perovskite QDs (ff_{QD}). As the porous matrix can be analyzed independently⁴⁶ before infiltrating the QDs, ff_{SiO_2} could be set at 0.51 and the (almost dispersion-less) refractive index of the solid part of the porous network at $N_{\text{SiO}_2} = 1.49$, as extracted by using a Cauchy model. Also, ff_{QD} could be experimentally determined by means of inductively coupled plasma optical emission spectrometry (ICP-OES) for each film, as

shown in Table S1 of the ESI,[†] where full details on this procedure can be found. Please note that the possibility to know the exact volume fraction and optical constants of the matrix, as well as the amount of nanocrystals present, implies a fundamental difference with respect to the optical analysis of the colloidal quantum dot solids. In the latter, the degree of interpenetration of the ligands surrounding the QDs is unknown, which prevents an accurate estimation of both the filling fraction and the optical constants of such organic networks, thus rendering the elucidation of the contribution of each one of the constituents to N_{eff} unfeasible.

Considering this information, a Kramers–Kronig consistent Forouhi–Bloomer dispersion model, in the Jobin Yvon parametrization (new amorphous),⁴⁷ was used to account for the spectral dependence of the complex refractive index of the QDs. To find the set of parameters that fit best the optical response of the fabricated films, we combined our optical model with a genetic algorithm. Fig. 3 shows the calculated specular reflectance (R), ballistic transmittance (T) and absorbance ($A = 1 - R - T$) spectra for the best fitting obtained for a bulk film and for a porous silica layer scaffold loaded with 2.2 nm MAPbBr₃ (Fig. 3a and c) and 6 nm MAPbI₃ (Fig. 3b and d) nanocrystals, along with their corresponding experimental spectra (the results for QDs of different sizes are provided in the ESI[†]). A fair agreement is found and the main spectral features are faithfully reproduced. The slight divergence observed in the reflectance background can be attributed to a small fraction of diffusely scattered light due to the roughness or imperfections

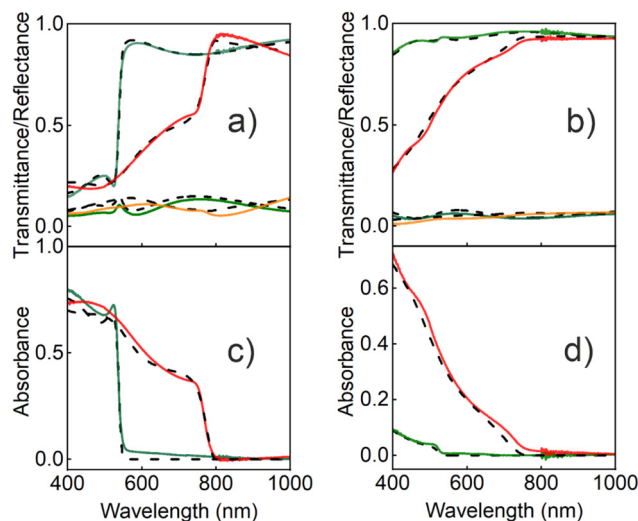


Fig. 3 (a) The transmittance and reflectance spectra recorded for MAPbBr₃ (light and dark green lines, respectively) and MAPbI₃ (red and orange lines, respectively) bulk films, and (b) the transmittance and reflectance spectra recorded for nc-MAPbBr₃@SiO₂ (light and dark green lines, respectively) and nc-MAPbI₃@SiO₂ films (red and orange lines, respectively). The absorbance spectra obtained from the R and T measurements ($A = 1 - R - T$) for (c) the MAPbBr₃ and MAPbI₃ bulk films (dark green and red lines, respectively) and (d) the MAPbBr₃ and MAPbI₃ nanocrystal films (dark green and red lines, respectively). In all graphs, dashed black lines indicate the corresponding theoretical fittings.



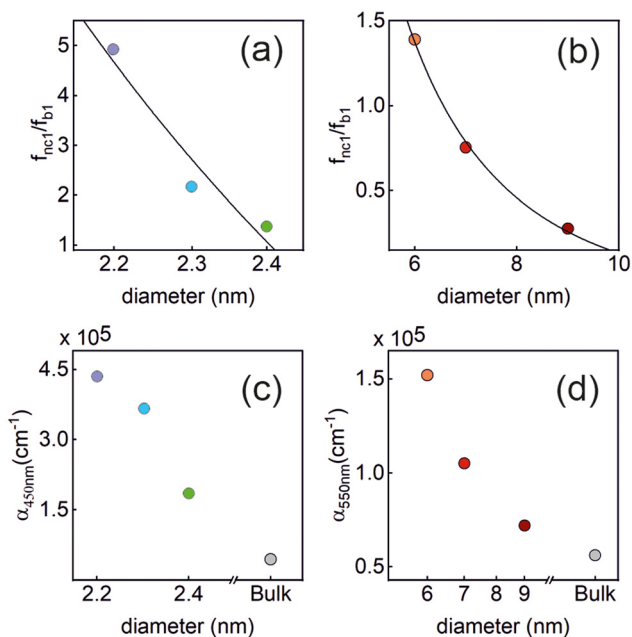


Fig. 5 Upper panels: the normalized oscillator strength of the first excitonic transition vs. the QD size, estimated for the (a) MAPbBr₃ QDs, and (b) MAPbI₃ QDs using the values of k extracted from our analysis. The solid line represents the theoretically expected $C(\frac{a\lambda}{r})^3$ dependence. Lower panels: the absorption coefficient α vs. the QD size estimated for the (c) MAPbBr₃ QDs (at $\lambda = 450$ nm), and (d) MAPbI₃ QDs (at $\lambda = 550$ nm). In each plot, the color code is the same as that shown in Fig. 2.

expected to become size independent.^{52,53} Our observations are at odds with this prediction, as shown in Fig. 5(c) and (d), in which we have plotted the absorption coefficient α for the MAPbBr₃ (at $\lambda = 450$ nm) and MAPbI₃ (at $\lambda = 550$ nm) QDs according to the following expression:

$$\alpha = \frac{4\pi k}{\lambda}. \quad (4)$$

One possible origin for this discrepancy may be that in our case the concentration is at orders of magnitude larger than those in the diluted dispersions (typically 10^{-6} M) commonly employed for this analysis, where QDs barely interact with each other. In our films, nanocrystals are close enough to allow a dot-to-dot charge transport.³⁵ Under these conditions, the neighbouring QDs are coupled through a dipolar interaction, which gives rise to an increase in the absorption cross section, and the polarization field induced by each nanoparticle may influence the surrounding nanoparticles. It has also been demonstrated that the dielectric confinement gives rise to an increase of the oscillator strength and therefore in the absorption cross section.⁵⁴ For instance, as a result of these interactions, it has been shown that QD solids made out of colloidal CdSe and PbS monolayers present an absorption increase as the size of the nanocrystals and ligands decreases.^{32,55} Also, composite nanostructures that resemble those herein studied show an increase in the absorption of the

QDs embedded in matrices with a lower dielectric constant, such as PbS in a glass matrix,⁵⁶ PbS/FAPI systems⁵⁷ and CsPbBr₃ NCs embedded in a Cs₄PbBr₆ matrix.⁵⁸

Conclusion

Herein, we demonstrate a method to determine the complex refractive indexes of MAPbBr₃ and MAPbI₃ perovskite quantum dots. To the best of our knowledge, the results attained constitute the first set of optical constants that can be considered intrinsic to these nanosized semiconductors. This achievement was possible due to the precise knowledge of the nanocrystal dielectric environment, which could be seized due to both the absence of capping ligands and the possibility to extract independently the optical constants of the host matrix in which the embedded nanocrystals are synthesized. We use a Kramers–Kronig consistent model to account for the spectral dispersion of the complex refractive index of the nanocrystals and an effective medium approximation approach to consider the effect of the porous silica matrix in which the nanocrystals are dispersed. Hence, contributions from the host and guest could be differentiated. Our analysis consistently reveals a remarkable increase of the values of both the real and the imaginary parts of the refractive index as the size of nanocrystals reduces. While the increase of the oscillator strength of the first excitonic transition grows according to the theoretical predictions; the behavior at energies well above the band gap edge is anomalous, but characteristic of QDs embedded in a vitreous host. We believe our results are both relevant from a fundamental perspective, as they provide a deeper insight into the origin of the remarkable optical properties of lead halide perovskites, and useful from an applied point of view, since they will allow a finer design and optimization of the optoelectronic devices in which perovskite QDs are already widely used.

Methods

Perovskite@SiO₂ composite preparation

The porous SiO₂-based thin film consists of a stratification of Ludox TMA nanoparticles (30 nm) deposited by dip-coating onto a microslide glass substrate up to a 400 nm thickness with a final calcination step (400 °C). The MAPbX₃ precursor solution contains a mixture of MAX and PbBr₂ or PbCl₂ (where X is Br or I), respectively, for bromide and iodide perovskites. Precursors were dissolved in *N,N*-dimethylformamide at a molar ratio of 3 to 1. Typically, for each case, the same recipes are employed for the preparation of the corresponding polycrystalline films, depositing the most concentrated precursor solution on the substrate, without the SiO₂ porous layer. NC synthesis is a one-pot process conducted in a glovebox, in which the precursor solution (different concentration for each NC) is dropped on top of the silica matrix and spin coated. Finally, the composite is heated up to 100 °C for 40 min.



Structural characterization

Lead determination was carried out by atomic emission spectroscopy with an inductively coupled plasma (ICP OES JASCO FT/IR-6200 IRT-5000). The microscopic analysis illustrated in Fig. 1 was performed using a FEI Talos F200S scanning/transmission electron microscope to observe the sample lamellae prepared by means of a focused ion beam (FIB, Carl Zeiss Auriga). For the composite thickness measurements, we used a profilometer.

Optical characterization

The photoluminescence spectra were recorded using a spectrophotometer, using two different lasers at 450 nm and 530 nm for the excitation of MAPbBr₃ and MAPbI₃, respectively. The R_T and T_T measurements were carried out inside an integrating sphere (DRA-2500, Agilent) connected to a commercial spectrophotometer (Cary 5000 UV-Vis-NIR). For the angular characterization, we made use of an accessory of the spectrophotometer, which is the Universal Measurement Accessory, allowing the analysis of the angular optical response of the composite films.

Complex refractive index determination

We fitted the optical response of the layers using an optical model based on the transfer matrix formalism. To model the spectral dependence of the nanocrystals, we used the Forouhi–Bloomer model in the Jobin–Yvon parametrization. Specifically, we considered three oscillators for MAPbI₃ and two oscillators for MAPbBr₃. Besides, we used an effective medium approximation to model the effective refractive index of the porous silica layer in which nanocrystals were embedded. A genetic algorithm was used to look for the parameters that provide the best fit for the experimental data. The results are shown in the ESI.†

Data availability

Data for this paper are available at Digital CSIC at <https://doi.org/10.20350/digitalCSIC/14799>. The code for estimating the optical constants of an arbitrary layered optical material may be found at <https://github.com/Multifunctional-Optical-Materials-Group>.

Conflicts of interest

There are no conflicts to declare.

Acknowledgements

Financial support from the Spanish Ministry of Science and Innovation under grant PID2020-116593RB-I00, funded by MCIN/AEI/10.13039/501100011033, and from the Junta de

Andalucía under grant P18-RT-2291 (FEDER/UE) is gratefully acknowledged.

References

- 1 J. I. Cisneros, Optical characterization of dielectric and semiconductor thin films by use of transmission data, *Appl. Opt.*, 1998, **37**, 5262–5270.
- 2 D. Poelman and D. F. Smet, Methods for the determination of the optical constants of thin films from single transmission measurements: a critical review, *J. Phys. D: Appl. Phys.*, 2003, **36**, 1850.
- 3 I. Moreels, K. Lambert, D. De Muynck, F. Vanhaecke, D. Poelman, J. C. Martins, G. Allan and Z. Hens, Composition and Size-Dependent Extinction Coefficient of Colloidal PbSe Quantum Dots, *Chem. Mater.*, 2007, **19**, 6101–6106.
- 4 I. Moreels, K. Lambert, D. Smeets, D. De Muynck, T. Nollet, J. C. Martins, F. Vanhaecke, A. Vantomme, C. Delerue, G. Allan and Z. Hens, Size-Dependent Optical Properties of Colloidal PbS Quantum Dots, *ACS Nano*, 2009, **3**, 3023–3030.
- 5 Z. Hens and I. Moreels, Light absorption by colloidal semiconductor quantum dots, *J. Mater. Chem.*, 2012, **22**, 10406–10415.
- 6 Y. C. Liu, J. H. Hsieh and S. K. Tung, Extraction of optical constants of zinc oxide thin films by ellipsometry with various models, *Thin Solid Films*, 2006, **510**, 32–38.
- 7 R. Kerremans, C. Kaiser, W. Li, N. Zarrabi, P. Meredith and A. Armin, The Optical Constants of Solution-Processed Semiconductors—New Challenges with Perovskites and Non-Fullerene Acceptors, *Adv. Opt. Mater.*, 2020, **8**, 2000319.
- 8 M. S. Alias, I. Dursun, M. I. Saidaminov, E. M. Diallo, P. Mishra, T. K. Ng, O. M. Bakr and B. S. Ooi, Optical constants of CH₃NH₃PbBr₃ perovskite thin films measured by spectroscopic ellipsometry, *Opt. Express*, 2016, **24**, 16586–16594.
- 9 Y. Jiang, M. A. Green, R. Sheng and A. Ho-Baillie, Room temperature optical properties of organic–inorganic lead halide perovskites, *Sol. Energy Mater. Sol. Cells*, 2015, **137**, 253–257.
- 10 P. Loeper, M. Stuckelberger, B. Niesen, J. Werner, M. Filipic, S. J. Moon, J. H. Yum, M. Topic, S. De Wolf and C. Ballif, Complex Refractive Index Spectra of CH₃NH₃PbI₃ Perovskite Thin Films Determined by Spectroscopic Ellipsometry and Spectrophotometry, *J. Phys. Chem. Lett.*, 2015, **6**, 66–71.
- 11 A. M. A. Leguy, P. Azarhoosh, M. I. Alonso, M. Campoy-Quiles, O. J. Weber, J. Yao, D. Bryant, M. T. Weller, J. Nelson, A. Walsh, M. Van Schilfhaarde and P. R. F. Barnes, Experimental and theoretical optical properties of methylammonium lead halide perovskites, *Nanoscale*, 2016, **8**, 6317–6327.
- 12 C. He, G. Zha, C. Deng, Y. An, R. Mao, Y. Liu, Y. Lu and Z. Chen, Refractive Index Dispersion of Organic–Inorganic



